Collective excitations in liquid methanol studied by coherent inelastic neutron scattering

1990 J. Phys.: Condens. Matter 2 6659

(http://iopscience.iop.org/0953-8984/2/31/019)

J. Phys.: Condens. Matter 2 (1990) 6659–6672. Printed in the UK

Collective excitations in liquid methanol studied by coherent inelastic neutron scattering

F J Bermejo†, F Batallan‡, J L Martinez§, M Garcia-Hernandez‖ and E Enciso¶

† Instituto de Estructura de la Materia, CSIC, Serrano 119, Madrid, E-28006, Spain
‡ Departamento de Fisica de Materiales, Facultad de Fisica, Universidad Complutense, E-28040, Madrid, Spain
§ Institut Laue–Langevin, 156X, F-38042, Grenoble Cédex, France
‖ ISIS Pulsed Neutron Facility, Rutherford Appleton Laboratory, Chilton, Didcot, Oxon OX11 0QX, UK
¶ Departamento de Quimica-Fisica, Facultad de Quimica, Universidad Complutense, E-28040, Madrid, Spain

Received 1 February 1990, in final form 27 April 1990

Abstract. Inelastic spectra of deuteromethanol measured by triple-axis neutron spectroscopy at several temperatures within the liquid range are reported. The observed scattering intensities are analysed in terms of reconstructions of the dynamical structure factor after deconvolution from instrumental effects, as well as model fits to the measured intensities. The data indicate the existence of a propagating high-frequency excitation, which at $T =$ 200 K becomes overdamped for wavevectors $Q > 0.6$ Å^{-1}. An insight into the nature of the observed excitation is given by the temperature behaviour of the damping factors. Such a trend gives additional support to the assignment of the excitation to closely packed patches of hydrogen-bonded molecules.

1. Introduction

The nature of high-frequency (of the order of a few terahertz) collective excitations in liquid matter is still a controversial topic in condensed matter physics.

Although the existence of well resolved Brillouin–Mandelstamm inelastic peaks is well known in most liquids for wavevectors up to several hundredths of a reciprocal angstrom and can be assigned to the propagation of hydrodynamic sound, the damping associated with those excitations (about 1 GHz in width) seemed to preclude experimental observation of such excitations in the kinematic range accessible to conventional neutron spectroscopy (wavevectors of about 1 Å^{-1} = 10 nm^{-1}).

However, clear evidence of well resolved inelastic peaks in neutron experiments on some liquid metals (see for instance [1] has made the subject an active area of research since the mid-1970s [2]. A debate has taken place concerning the physical meaning of such excitations since at those wavevectors they cannot be consistently assigned to the propagation of hydrodynamic sound.

From theoretical standpoints, attempts have been made towards analysis of such phenomena either in terms of phenomenological extrapolations of the 'generalised hydrodynamics' (GH) type [3] or from full kinetic theories (KT) (see for example [4])

0953-8984/90/316659 + 14 $03.50

within which the recent successes of several families of 'mode-coupling' approximations are outstanding (for a concise introduction see [5]).

In both cases predictions of something analogous to a dispersion relation in a solid are made. The characteristic that differentiates the predictions made by both series of approaches is the nature of such high-frequency modes. So, the GH theories predict the appearance of a 'positive dispersion' phenomenon (i.e. the hydrodynamic sound is approached from high frequencies as the wavector is decreased), which is able to explain the relatively high frequencies of the observed excitations, whereas the appearance of a new, high-frequency mode of a distinctive physical origin (i.e. supported by a specific physical process that depends upon the system under study) is postulated by recent KT developments.

In order to contrast the validity of the approximations mentioned above, a consistent set of experimental measurements becomes necessary. However, apart from the results in liquid metals and molten salts [6], there is a wealth of experimental data for liquified rare gases [7], where the inelastic peaks are only resolved at rather low wavevector values (0.1 Å^{-1}).

On the other hand there is a wealth of computational (molecular dynamics) evidence indicating the existence of this kind of mode for systems interacting through Lennard–Jones [3, 8] or more complex potentials, the case of liquid water being paramount [9].

Although two independent neutron scattering experiments have been reported for the latter case, it is difficult to draw any definite conclusion since, apart from being performed under rather different experimental conditions, the analysis of the weak signals has been carried out in a way that makes a comparison between both results difficult [10, 11].

The purpose of this work is to contribute to clarifying the present debate by analysing the spectra of collective excitations in liquid deuterated methanol (CD_3OD). The reasons behind such a choice are twofold. First, the molecule can be considered as a structural analogue of water, where one of the deuterons has been replaced by an inert CD_3 group. Such a substitution is believed to have strong implications on the hydrogen bond network, which is now constituted by long chains [12], which makes the bonding net more amenable to modelling than the case of water because of the complex intermolecular structures in this latter case. On the other hand, although the molecular unit is comparatively more complex than water, the inelastic intensity arising from individual modes (molecular rotations and translations) can be substantially reduced compared to water, because of the low melting point of the alcohol (190 K) and larger mass. Previous quasi-elastic studies [13, 14] have shown that the linewidth of the central elastic component can be reduced to $\simeq 10^{-3}$ THz at $T = 200$ K, and that the weak rotational components associated with molecular and methyl group reorientations will contribute to a weak inelastic background with linewidths of 0.08 and 0.5 THz, respectively. Such a fact would eliminate the uncertainties of the previous experiments on water where the observed spectra contain quasi-elastic contributions two orders of magnitude larger, thus complicating the separation of individual and collective modes.

An additional motivation for choosing this material was the fact that at $T = 200$ K results from computer simulation indicate that the lifetime of the excitation should be long enough to be resolved in conventional neutron spectroscopy [15], which in conjunction with the very narrow elastic component would render the inelastic peaks easy to identify.

The experimental and data treatment details will be presented in section 2. The interpretation of the observed spectra as well as their behaviour with varying tem-

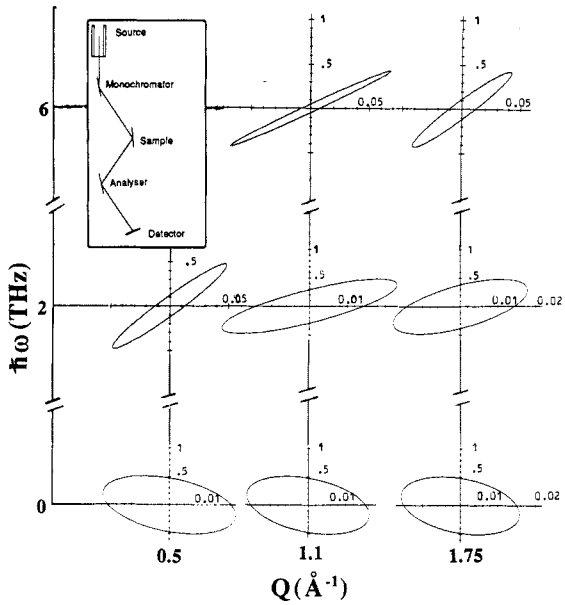

Figure 1. Resolution ellipsoids for selected values of energy and momentum transfers. The inset shows the spectrometer configuration employed in the present experiments. Note the different scales within the ellipsoids.

perature will be described in section 3, and a comparison with the available results for water as well as a discussion of results are finally presented in section 4.

2. Experiments and data analysis

2.1. Experimental details

The experiments were performed using the triple-axis spectrometer IN8 located at one of the thermal neutron lines of the High-Flux Reactor of the Institut Laue-Langevin (Grenoble).

Since the measurements had to be carried out at rather low angles (close to the direct beam) restrictive collimations of 30′ (in pile), 20′ (monochromator and sample), 10′ (sample and analyser) and 40′ (analyser and detector) have to be used in order to reduce the contamination from the incident beam.

A cylindrical vacuum tank of 1 m diameter was mounted surrounding the cryostat tail in order to reduce diffuse scattering from the air. All scans were carried out in constant-Q mode with fixed incident wavevector $k = 6.2$ Å^{-1}, which corresponds to a neutron energy of 80 meV. For such a purpose, the (2 2 0) reflection of the copper monochromator was used and the (0 0 4) reflection of pyrolitic graphite focusing in the detector was used for the analyser. The momentum-transfer range explored in the present experiment was 0.35–2.2 Å^{-1}, which covers the region comprising the first liquid diffraction peak (about 1.8 Å^{-1}). Both energy gain and loss sides of the spectra were measured in all cases covering the allowed full kinematic range.

The spectrometer configuration described above (see inset of figure 1) gives an acceptable resolution in energy transfer as well as rather high resolution in momentum transfer. As an indication several $\Delta E/\Delta Q$ resolution ellipsoids are shown in figure 1.

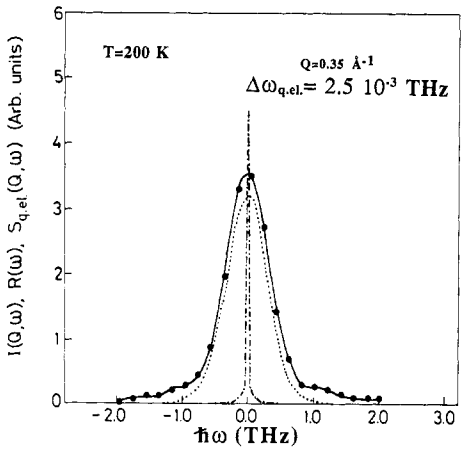

Figure 2. Representative spectrum for $Q = 0.35$ Å^{-1}. Full circles represent the experimental points; the full curve is a spline fit to those points. The measured resolution function corresponds to the dotted curve; and the chain curve gives the quasi-elastic component.

As can be seen, the resolution in energy transfer is in most cases about 0.7 THz, whereas values of the order of 0.02 Å^{-1} were computed for momentum transfers. As a consequence all the data analysis steps were carried out considering only instrumental effects for energy transfers.

The cell followed a design already used for one of the measurements on lead [16]. It has been built as a box of 55 mm height, 33 mm width and 6 mm thickness containing horizontal plates of cadmium-coated aluminium of 0.1 mm thickness separated by 1 mm in order to reduce to a minimum the contribution of multiple scattering.

Several runs were carried out using the empty cell, which scatters about 2% of the total intensity, and this contribution was subtracted.

The temperature was controlled using a standard 'orange' cryostat with a regulation better than 0.3 K. Most of the runs were performed at $T = 200$ K, and some spectra for several selected Q-values were also carried out at $T = 250$ and 300 K.

The instrumental slit (resolution) function was measured using a vanadium standard, which gave a full-width at half-maximum (FWHM) of about 0.6 THz.

2.2. *Data analysis*

In order to illustrate the difficulties of isolating the $S(Q, \omega)$ dynamic structure factors from the observed intensities, figure 2 depicts one of the measured spectra as well as the experimental resolution function and an indication of the relative width of the central, quasi-elastic $R_{qe}(Q, \omega)$ response.

As can be seen upon inspection of the figure, although there are some hints of inelastic peaks centred about 1 THz, their weak intensity makes a proper account of the resolution effects necessary. In such respects, the deconvolution of the spectra in order to obtain an estimate of the underlying $S(Q, \omega)$ seems to be an adequate first step of the analysis for the following reasons: (i) it will provide a model-free estimation of the dynamic structure factor, which can be compared in a later stage to model-dependent fits; (ii) it seems clear upon inspection of the raw spectra shown in figure 3 that, since all the relevant information is contained in the weak wings of the spectra, any fitting procedure will be insensitive to small changes in intensity in that region unless substantial prior knowledge is introduced. The deconvoluted spectra should then also serve to set limits on model-dependent parameters, as will be described in a later section.

A deconvolution algorithm of the MaxEnt [17] type was chosen for the purpose since it is known to provide reliable results in other branches of physics where the estimations have to be done under somewhat similar conditions (see e.g. [18]).

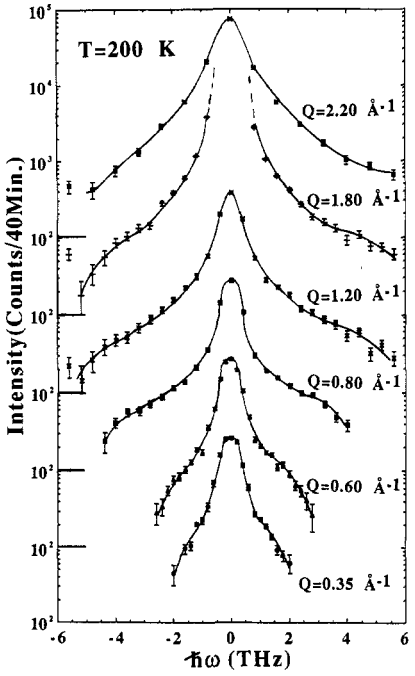

Figure 3. Log[$I(Q, \omega)$] (raw data): full curves are spline fits and are given as a guide for the eye.

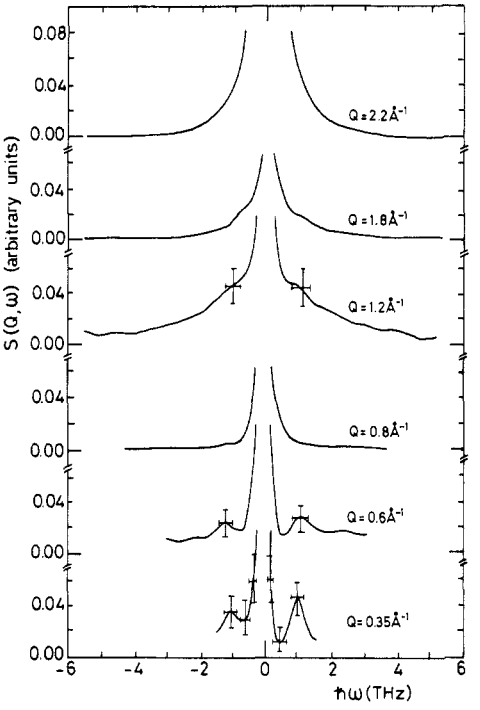

Figure 4. Deconvoluted spectra (reconstructed $S(Q, \omega)$). The central, elastic peak is a quasi-elastic component with widths (estimated after the deconvolution) of about 0.05 THz. The error estimates (crosses) were computed using the procedure described in the appendix.

The deconvolution procedure makes use of the Cambridge package [19], and was constructed following lines analogous to those described in [20].

A prior estimate of $S(Q, \omega)$ has to be introduced as previous knowledge. For such a purpose the previously measured quasi-elastic response $R_{qe}(Q, \omega)$ has been used. Once folded with the measured $O(\omega)$ resolution function, this contribution takes into account most of the spectral intensity within $-0.6\ \text{THz} < \hbar\omega < 0.6\ \text{THz}$. The choosing of such *a priori* information is tantamount to assuming a flat spectrum for the collective oscillations. Furthermore, the width of the strong, central component of the unfolded spectrum can be used as an estimate of the reliability of such a prior distribution since the recovered magnitude should be comparable to the one used as a prior (of the order of some hundredths of terahertz).

A set of deconvoluted spectra corresponding to those shown in figure 3 are depicted in figure 4, and further discussion will be deferred to section 4.

In order to assess the statistical significance of the deconvoluted spectra, the confidence limits have been computed by means of an adaptation of the Backus–Gilbert [21] method along similar lines as those used for the computation of such quantities in the inversion of liquid and amorphous static structure factors [20].

In the above-mentioned scheme estimates for the confidence intervals for both energy transfer and intensity can be computed following the procedure given in the appendix.

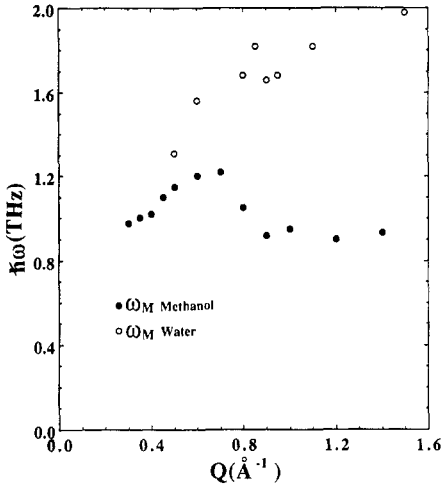

Figure 5. Position of the maxima of the reconstructed $S(Q, \omega)$ versus Q. For momentum transfers larger than $0.7\ \text{Å}^{-1}$ the quantities $\omega^2/Q^2S(Q, \omega)$ are plotted. The full circles represent the measurement of water reported in [10].

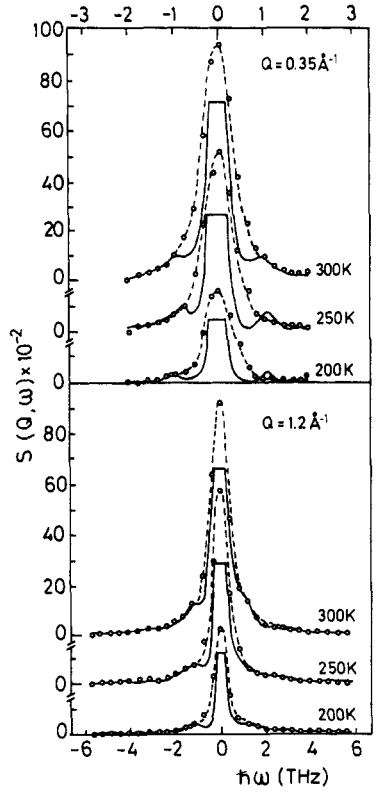

Figure 6. Temperature dependence of the spectra. The upper part of the graph shows spectra for $Q = 0.35\ \text{Å}^{-1}$ and the lower for $Q = 1.2\ \text{Å}^{-1}$. The open circles represent the measured data and the full curves (truncated at the elastic energy transfer value) are the deconvoluted spectra.

3. Results

3.1. Estimates of the dynamical structure factor

Several features are clearly visible from the set of deconvoluted spectra. In the first place, distinctive side peaks are clearly seen up to a Q-value of $0.6\ \text{Å}^{-1}$. From $Q = 0.9\ \text{Å}^{-1}$ onwards the excitation becomes overdamped, so that only a broad component with the central component superimposed on it is shown. The apparent width of the overdamped mode get substantially reduced when approaching $Q = 1.8\ \text{Å}^{-1}$ (i.e. the maximum of the $S(Q)$ static structure factor). In order to explore the possible existence of a 'dispersion relation', the position in energy of the maxima of the inelastic side peaks versus momentum transfers has been drawn in figure 5. In order to locate that value in the spectra within the overdamping region, the quantity $\omega^2/Q^2S(Q, \omega)$ was computed. This function, which can be related to the longitudinal current correlation function, always shows side peaks located at frequencies $\omega_M(Q)$. Although such frequencies cannot be identified with the true physical frequency of the excitation, since the damping shifts the maximum from the true ω_j value, they provide a first approximation valid to explore the spatial dispersion of the excitation. On the other hand, such a function

can be readily compared with the one reported for water [10], also derived after a deconvolution procedure, as is also done in figure 5.

In order further to ensure the physical significance of the reconstructed structure factors, their behaviour with temperature was also studied. Several spectra for two different Q-values and temperatures of 200, 250 and 300 K as well as their deconvoluted counterparts are shown in figure 6. What can be clearly seen from the figure is the fact that increasing the temperature substantially broadens the spectra as well as introduces a larger inelastic background due to the increased population of the excitations. Furthermore, what also becomes clear from the deconvoluted spectra is the fact that the damping at 300 K seems to be large enough that the side peaks at $Q = 0.35$ Å^{-1} are now barely resolved.

It is also worth noting that the increase in damping with respect to increasing temperature gives further support to the hypothesis of a distinctive nature of these excitations with respect to those measurable in the long-wavelength regime. A recent light-scattering experiment [22] has shown that the sound damping coefficient (related to the widths of the Brillouin lines) exhibits a complicated dependence on the temperature. If the nature of those hydrodynamic excitations and the present ones were the same, one should expect an analogous behaviour with temperature, which runs counter to the present experimental evidence.

3.2. *Analysis in terms of model functions*

The purpose of this section is to compare the results obtained in the previous part with those derived from fits to the observed intensities in terms of theoretical models.

The procedure to follow involves the specification of a function $R_{\mathrm{mod}}(Q, \omega)$ in terms of a set of model parameters so that the intensities to be compared with the measured ones are computed from

$$I_{\mathrm{mod}}(Q, \omega) = \{S_{\mathrm{cm}}(Q) \exp(-\mu Q^2)[R_{\mathrm{mod}}(Q, \omega) + R_{\mathrm{qe}}(Q, \omega)]\} * O(\omega)$$

where the subscript cm denotes the structure factor for molecular centres, the exponential is a Debye–Waller term with amplitude μ, the symbol $*$ stands for convolution and $O(\omega)$ is the measured slit (resolution) function. The $S_{\mathrm{cm}}(Q)$ can be derived from computer simulations or can be obtained from the observed structure factor in diffraction experiments (an example will be given further on). The mean square amplitude entering the Debye–Waller term may be derived from previous quasi-elastic measurements or estimated from the intensity versus Q behaviour of the central elastic peak. Finally, as was mentioned above, the central quasi-elastic response function is constructed from data derived from a previous low-energy study [13], where the effects of molecular rotations and centre-of-mass motions are taken into account in an explicit way.

The first model to be considered is of linearised hydrodynamics nature [2], and therefore it represents a rather sweeping approximation. Its limit of validity extends to the momentum-transfer value where the sound damping becomes comparable with the frequency $v_0 Q$, where v_0 stands for the adiabatic sound velocity. Apart from heuristic reasons, we have performed some fits using this model since the most recent experiment on water was done along similar lines [11]. The model is then specified in terms of a harmonic frequency ω_j and a damping factor Γ_j, which represents the motion of a damped harmonic oscillator

$$R_{\mathrm{mod}}(Q, \omega) = \frac{B\omega[1 + n(\omega)]\Gamma_j}{(\omega^2 - \omega_j^2)^2 + (\Gamma_j \omega)^2} \qquad B = \frac{1}{kT}$$

where the first term in brackets represents a Bose occupation factor.

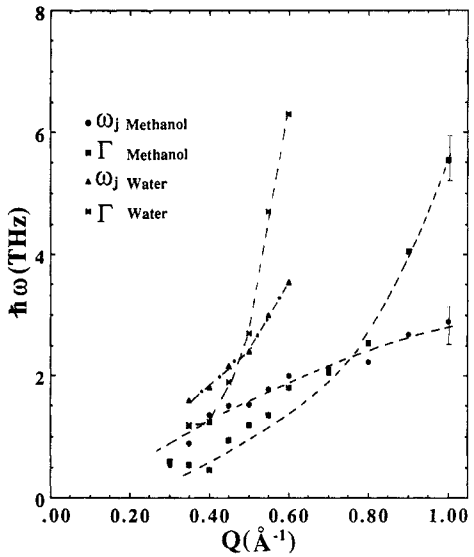

Figure 7. Harmonic frequency and damping factor versus momentum transfer for the hydrodynamic (damped oscillator) model. The full circles and squares represent similar quantities corresponding to water, taken from [11]. The error bars represent one standard deviation.

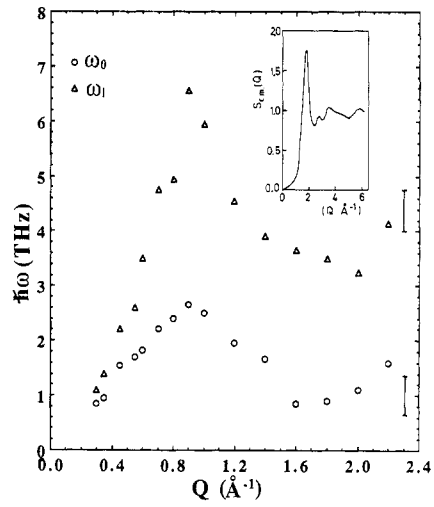

Figure 8. Square roots of the normalised frequency moments derived from fits using the viscoelastic model. The bar shown in the lower right-hand side gives the estimated error bar, which is about the same magnitude for the explored Q-range. The inset shows the molecular-centres structure factor $S_{cm}(Q)$ computed for $T = 200$ K from a molecular dynamics simulation [15].

This model represents a generalisation for molecular liquids of the one currently used for atomic fluids [2] since the central (Rayleigh) peak has been replaced by the quasi-elastic response function.

It has to be emphasised that the only reliable range where physically sound results can be obtained using this model is limited not only by the condition mentioned above but also by the fact that when the mode becomes overdamped only the ratio between ω_j and Γ_j can be safely estimated from the measured intensities.

The derived harmonic frequencies and damping factors are given in figure 7 for a momentum transfer up to 1.0 Å^{-1}.

The second model that we have used is based upon viscoelastic approximations [2] that constitute a variant of the family of GH theories. As such, it extends its range of validity towards the kinetic region, and constitutes an adaptation of the well known three-pole formula [23] where the quasi-elastic contribution has been added in a heuristic way, the reason for it being the inadequate Q dependence of the thermal mode predicted by the viscoelastic theory. As can be seen from data derived from this model, the width of the thermal peak built-in in the viscoelastic theory only amounts to a few gigahertz in all the kinematic range explored in the present experiment, so that it can be safely replaced by the measured quasi-elastic response.

The relevant quantities in this case are the normalised second and fourth frequency moments of the dynamical structure factor. The model then reads

$$R_{\text{mod}}(Q, \omega) = [1 + n(\omega)] \frac{\omega_0^2(\omega_1^2 - \omega_0^2)\tau}{[\omega\tau(\omega^2 - \omega_1^2)]^2 + (\omega^2 - \omega_0^2)^2}$$

with

$$\omega_0^2 = \int d\omega\, \omega^2 S(Q, \omega) \Big/ \int d\omega\, S(Q, \omega)$$

$$\omega_1^2 = \int d\omega\, \omega^4 S(Q, \omega) \Big/ \int d\omega\, \omega^2 S(Q, \omega)$$

where the relaxation time is given in terms of both normalised frequency moments ω_0^2 and ω_1^2, and the relaxation (Maxwell) time is given by

$$\tau^{-1} = 2[(\omega_1^2 - \omega_0^2)/\pi]^{1/2}$$

following the simplified viscoelastic approximation [2]. It is worth emphasising that therefore the model is specified in terms of only two free parameters, ω_0^2 and ω_1^2, which must follow predetermined sum rules.

The fitted frequency moments are given in figure 8 for the whole momentum-transfer range explored in the present experiments.

Both models are able to fit the spectra and, as expected, become nearly equivalent at low Q. However, beyond $Q = 0.6$ Å^{-1} the hydrodynamic model cannot provide sound physical information since: (i) its validity only extends up to a momentum transfer $Q \simeq v_0/\Gamma_j$ [23]; and (ii) when the damping constant greatly exceeds the value of the harmonic frequency, only the ratio ω_j/Γ_j can be safely estimated from the measured spectra.

4. Discussion

From comparison of the results shown in figures 7 and 8 several qualifications can be pointed out. First, the harmonic frequency ω_j specified in the linearised hydrodynamics model and the ω_0 moment derived from the viscoelastic approximation are nearly coincident at low Q-values. It is worth noting that, in the long-wavelength limit, the viscoelastic model gives

$$\lim_{Q \to 0} \omega_0 = Q v_T$$

where v_T is the isothermal sound velocity (related to the adiabatic velocity $v_0 = \gamma v_T$), and therefore, for a value of the ratio of specific heats, γ, not too different from one, the same values for the two magnitudes should be recovered from the two models.

An extrapolation towards $Q \to 0$ of either ω_j or ω_0 gives a value of 2450 ± 215 m s^{-1}, which is well above the velocity of sound measured in a recent light-scattering experiment (1460 m s^{-1}).

It is obviously difficult to decide whether this velocity arises from a high-frequency excitation specific to multicomponent fluids as proposed in [9, 24] or whether it is simply a continuation to larger momentum transfers of ordinary sound (positive dispersion) as predicted by most of the GH approaches. Computer molecular dynamics simulations are being carried out with the hope of getting some additional information to clarify this disagreement.

Secondly, the ω_1 normalised fourth frequency moment comprises two contributions of thermal and sound propagation nature respectively. If the former one is neglected (at $T = 200$ K the thermal contribution $(\gamma - 1)\lambda/C_p = 3.13 \times 10^{-5}$ N s m^{-2}, i.e. two orders of magnitude smaller than the elastic constants contributions), one should recover from the low-Q limit of ω_1 a quantity given in terms of the instantaneous shear (G_∞) and bulk (K_∞) rigidity moduli

$$v_\infty = \lim_{Q \to 0} \omega_1 = (\tfrac{4}{3} G_\infty + K_\infty)/\rho$$

where ρ represents the mass density. Therefore, in such a limit ω_1 may be interpreted

as a high-frequency velocity representing purely elastic propagating waves. The value obtained from extrapolation to $Q \rightarrow 0$ of the ω_1 values (up to 0.4 Å^{-1}) gives a high-frequency velocity v_∞ of 3298 ± 183 m s^{-1}. As a consequence, it becomes clear that the value of 2450 m s^{-1} obtained from extrapolation of the low-Q data can be accommodated within the viscoelastic framework as arising from the high-frequency processes built in through the incorporation of wavevector-dependent elastic constants.

A comparison between the two models regarding the damping terms can also be performed. For such a purpose, one should recall that the damping constant Γ_j obtained from the fits of the hydrodynamic model may be related to the damping derived from the application of the viscoelastic approximation since for γ values close to one [23] the following equality

$$2\Gamma_j = \lim_{Q \to 0} \frac{(\omega_1^2 - \omega_0^2)}{Q} \tau$$

should be valid.

From comparison of the results given for the damping terms in figures 7 and 8, it becomes clear that the damping constant obtained from the viscoelastic model does not reproduce the values computed from the linearised hydrodynamics model, since values for the damping well above the harmonic frequencies are predicted for the available Q-range. In order to clarify this disagreement, it is worth comparing the limits given by the two models beyond which the mode becomes overdamped (no structure in ω). The usual criteria to give a lower bound to the underdamped zone are

$$2\omega_j^2 > \Gamma_j^2 \qquad \text{(hydrodynamic)}$$

$$3\omega_0^2 > \omega_1^2 \qquad \text{(viscoelastic)}.$$

From inspection of figures 7 and 8 it is easily seen that such limits are $Q = 0.8$ Å^{-1} for the hydrodynamic model and $Q = 0.55$ Å^{-1} for the viscoelastic one. At this point it is helpful to re-examine figure 4, which displays some of the deconvoluted spectra.

Although it is obviously difficult to make a quantitative comparison of the structure factors displayed in the figure, let us assume as a criterion to set the boundary of the underdamped zone the appearance of side structures for both creation and annihilation sides of the spectra. As a result it may be inferred that such a boundary has to be about $Q = 0.6$ Å^{-1}, which is in reasonable agreement with the results obtained from the viscoelastic model. It is difficult to ascertain the reasons for such discrepancy with the hydrodynamic result since, as already mentioned, reasons of both physical and numerical stability can contribute to it.

The ω_m peak maxima shown in figure 5 may be interpreted with reference to the two models since the peak maxima should then be

$$\omega_M = (\omega_j - \Gamma_j^2/2) \qquad \text{(hydrodynamic)}$$

$$\omega_M = (1/3)^{1/2}\{2\omega_1^2 - \tau^{-2} + [\omega_1^4 + \tau^{-4} - 2\tau^{-2}(2\omega_1^2 - 3\omega_0^2)]\}^{1/2} \qquad \text{(viscoelastic)}.$$

Therefore, if, for the sake of simplicity, we analyse the ω_M dispersion in terms of the two models, taking the fitted values for ω_j or ω_0 and ω_1, we can get an estimate of the departure of the deconvoluted spectra from the ones given in terms of the model functions.

For the damped oscillator case, damping parameters of $\Gamma = 0.26$ THz at $Q = 0.35$ Å^{-1} and 1.06 THz at $Q = 0.6$ Å^{-1} are obtained from values of the fitted frequencies taken from figure 7 and values of ω_M peak maxima taken from figure 5. As can be easily

shown by inspection of figure 7, although the damping at $Q = 0.35$ Å^{-1} is in agreement (within error bars) with the fitted one, the value recovered at $Q = 0.6$ Å^{-1} is significantly smaller than the one resulting from the parametric fit (1.8 THz). On the other hand, if the values for ω_0 and ω_1 are used to calculate the position of the peak maxima, values of 1.22 and 1.33 THz are obtained for the same momentum-transfer values. Although these latter values are slightly larger than the ones given in figure 5, they seem to reproduce the shape of the ω_M versus Q curve, for the range of momentum transfers where the excitations are not overdamped.

The estimates of the relaxation times arising from the fits using the viscoelastic model are about 0.34 ps for $Q = 0.35$ Å^{-1} and 3.45 ps for $Q = 0.9$ Å^{-1} (i.e. the maximum of the 'dispersion relation'). Such values are well below the one estimated for the longitudinal viscosity in a previous light-scattering experiment, where it was found that at 200 K the relaxation time was about 33 ps.

Finally, it is worth comparing the present results with those already published for liquid water. As the reader may have already noted, both figures 6 and 7 depict data taken from [10] and [11], which are directly comparable to the ones given in this work since they have been obtained following the same lines of treatment.

The shapes of the curves depicting the values of the maxima of the side peaks of the deconvoluted spectra for heavy water and the present experimental results are remarkably similar, although the limited Q-range available in the experiment reported in [10] precludes any detailed comparison.

The curves obtained in [11] using the same incident energy are plotted in figure 7. No comparison is possible in terms of the viscoelastic model since no data have been reported following such an analysis.

5. Conclusions

The work reported herein shows that coherent inelastic neutron scattering spectra from molecular liquids can be safely analysed if several independent approaches are taken concurrently. The dangers associated with conclusions derived from one single analysis in terms of a model function can be substantially minimised if some estimate of the $S(Q, \omega)$ structure factor free from instrumental effects is available.

The discrepancies between data obtained from fits to different models to the observed intensities can be taken into account if one considers their limits of validity.

The data reported here indicate that the relatively high frequency of the observed mode with respect to hydrodynamic sound may well be explained in terms of a 'positive dispersion' predicted by the GH theories, although the assignment of it to a new mode cannot be ruled out.

The temperature behaviour of the apparent width of the excitation constitutes a distinctive characteristic of these modes, since it substantially differs from what is observed in the long-wavelength region [23]. Such a fact lends further support to the hypothesis that sustains that such a mode is originated by highly packed hydrogen-bonded patches of molecules, mainly composed of linear chains. Since the lifetime of one hydrogen bond in liquid methanol seems to decrease with temperature [12, 14], it seems clear that, on qualitative grounds, the lifetime of the excitation should also decrease with increasing temperature, which is in agreement with the results reported in this work.

The magnitude of the relaxation times derived from the analysis in terms of the viscoelastic model (about 1 ps) lends further support to the idea of assigning the observed

mode to fluctuations in the microscopic hydrogen-bond structure. In such a respect, the estimates of the hydrogen-bond lifetime of 2 ps made in [12] for $T = 298$ K and the recent value of 5 ps derived from a previous quasi-elastic study [14] for $T = 200$ K seem to agree with what could be expected for an excitation sustained by chains of hydrogen-bonded molecules, coupled to a continuum characterised by a relatively large mass.

A comparison with already reported data for liquid water shows that the results from both measurements [10, 11] can be reconciled since the analyses were done in terms of the ω_M frequencies (peak positions of $S(Q, \omega)$) [10] or their ω_j counterparts [11]. Therefore the existence of a fast kinetic mode cannot be substantiated from such a comparison as done in [9]. In order to provide a more meaningful comparison, it would be worth analysing the available data for water under a simplified viscoelastic approximation as well as to carry out additional measurements under conditions more suitable for the separation of the collective mode from the quasi-elastic response.

Acknowledgments

Work supported in part by DGICYT (Spain), Grant no. PB86-0617-C02. Helpful discussions with Dr B Dorner from the ILL are acknowledged. Mr A Gomez gave us invaluable help during the preparation of the manuscript.

Appendix. Estimation of confidence limits for the deconvoluted spectra

In what follows we shall describe an adaptation of the method originally given by Backus and Gilbert [21], which has been applied before for the inversion of liquid and amorphous structure factors [20] and for the analysis of small-angle spectra [25]. For further references the interested reader should consult [26] and [27] (the latter contains a general introduction to the field).

The measured inelastic intensity at the ω_j energy transfer can be written as

$$I(Q, \omega_j) = \int S(Q, \omega) O(\omega_j - \omega)\, \mathrm{d}\omega \tag{A1}$$

where $S(Q, \omega)$ is the dynamical structure factor and $O(\omega)$ is a resolution (slit) function measured under ideal (no noise) conditions, which because of the high resolution in momentum transfers has been assumed to have a negligible Q dependence.

Let us assume as a model response function a harmonic oscillator with frequency ω_j

$$S_h(Q, \omega) = \omega[1 + n(\omega)]\delta(\omega \pm \omega_j)/\omega^2. \tag{A2}$$

The problem is then to obtain a good estimate for $S_h(Q, \omega)$ at a given point $\omega = \omega_j$.

Since the convolution operator is of linear type, we can write the estimator as a combination of the data

$$S_{est}(Q, \omega) = \sum_j a_j(\omega_0) I(Q, \omega_j) \tag{A3}$$

where the $a_j(\omega_0)$ coefficients are to be found. From (A1) we can see that

$$S_{est}(Q, \omega) = \sum_j a_j(\omega_0) \int S_h(Q, \omega) O(\omega_j - \omega)\, \mathrm{d}\omega = \int T(\omega_j - \omega) S(Q, \omega)\, \mathrm{d}\omega \tag{A4}$$

where

$$T(\omega_0, \omega) = \sum_j a_j(\omega_0) O(\omega) \tag{A5}$$

is a new resolution function given in terms of the theoretical (or the measured) resolution $O(\omega)$.

At this point we shall take into account the $e(\omega)$ measurement errors, which are given as variances in the intensity for each data point. We can then write the error in the sought $S_{\text{est}}(Q, \omega)$ estimate as

$$E(\omega) = \text{var}[S_{\text{est}}(Q, \omega)] = \sum_j a_j(\omega_0) e(\omega_j). \tag{A6}$$

Our purpose is to find estimates for confidence intervals in width (resolution) and intensity. For such a purpose we construct the functional

$$\Delta A + \lambda E(\omega) \tag{A7}$$

where

$$\Delta A = \int [T(\omega_0, \omega) - S_{\text{h}}(Q, \omega)] \, \text{d}\omega \tag{A8}$$

measures the deviation from the true spectrum and λ is an undetermined multiplier.

The $a_j(\omega_0)$ coefficients can be calculated by differentiation of (A7). A set of N simultaneous linear equations results, which can be solved for the $a_j(\omega_0)$. If we assume that the instrumental resolution is a Gaussian with width $\Delta\omega$, the set of equations thus becomes

$$\sum_j \left(\frac{2\pi^2 (\Delta\omega)^{1/4} (\omega_j + \omega_k)}{\exp\{-(\omega_j^2 + \omega_k^2) + [(\omega_j + \omega_k)/8]^2\}} + \lambda E(\omega) \right) \times a_j(\omega_0) - O(\omega_k, \omega)\delta(\omega - \omega_j) + 2\mu = 0. \tag{A9}$$

The $T(\omega_0, \omega)$ functions are computed for every ω_0 for several values of λ, once the $a_j(\omega_0)$ coefficients are known from solution of (A9). The width of such functions represents an estimate of the attainable resolution, which includes the effect of observational noise, and gives an indication of the confidence limit in energy transfers. Since the effect of the measurement noise is introduced by assigning different values for the λ multiplier, for every λ a pair of values of $T(\omega_0, \omega)$ and $E(\omega)$ is generated, the latter one giving an estimate of the error in the deconvoluted intensities. Both values are solutions of the variational problem (A7) and taking an optimum value for one of them implies a large uncertainty for the other. Therefore a compromise has to be found between acceptable resolution in energy and accuracy in the deconvoluted intensities. For such a purpose, a plot of the width of the $T(\omega_0, \omega)$ function versus $E(\omega)$ is then generated, which represents a curve defining a boundary where all the pairs of points with coordinate width $E(\omega)$ must lie. Such a curve is in most cases a closed one, from which estimates of confidence intervals for both resolution in energy transfers and intensities can be obtained from the lower left part of it.

References

[1] Copley J R D and Rowe J M 1974 *Phys. Rev.* A **9** 1656

[2] Lovesey S W 1986 *Theory of Thermal Neutron Scattering from Condensed Matter* (Oxford: Oxford University Press) ch 5

[3] Boon J P and Yip S 1982 *Molecular Hydrodynamics* (New York: McGraw-Hill)
[4] Hansen J P and McDonald I R 1986 *Theory of Simple Liquids* (New York: Academic) ch 9
[5] Sjölander A 1987 *Liquids and Amorphous Materials* (ed E Lüscher *et al*) NATO ASI E-118 (Dordrecht: Nijhoff) p 239
[6] Rovere M and Tosi M P 1986 *Rep. Prog. Phys.* **49** 1001
[7] de Schepper I M, van Rijs J C, van Well A A, Verkerk P, de Graaf L A and Bruin C 1984 *Phys. Rev.* A **29** 1602
[8] de Schepper I M, Cohen E G D, Bruin C, van Rijs J C, Montfrooij W and de Graaf L A 1988 *Phys. Rev.* A **38** 271
[9] Ricci M A, Rocca D, Ruocco G and Vallauri R 1988 *Phys. Rev. Lett.* **61** 1958; see also 1989 *Helv. Phys. Acta* **62** 676
[10] Bosi P, Dupre F, Mezinger F, Sacheti F and Spinelli M C 1978 *Lett. Nuovo Cim.* **21** 436
[11] Teixeira J, Bellisent-Funel M C, Chen S H and Dorner B 1985 *Phys. Rev. Lett.* **54** 2681
[12] Bertolini D, Cassettari M, Ferrario M, Grigolini P and Salvetti G 1985 *Adv. Chem. Phys.* **62** 277
[13] Bermejo F J, Batallan F, Enciso E, White R, Dianoux A J and Howells W S 1990 *J. Phys.: Condens. Matter* **2** 1301
[14] Bermejo F J, Batallan F, Howells W S, Carlile C J, Garcia-Hernandez M, Alvarez M and Alonso J 1990 *J. Phys.: Condens. Matter* in press
[15] Alonso J and Bermejo F J unpublished data
[16] Söderstrom O, Copley J R D, Suck J B and Dorner B 1980 *J. Phys. F: Met. Phys.* **10** L151
[17] Skilling J (ed) 1989 *Maximum Entropy and Bayesian Methods* (Dordrecht: Kluwer)
[18] Narayan R and Nityananda R 1986 *Annu. Rev. Astron. Astrophys.* **24** 127
[19] Skilling J and Bryan R K 1984 *Mon. Not. R. Astron. Soc.* **211** 111
[20] Bermejo F J, Mompean F J, Santoro J and Dore J C 1987 *Nucl. Instrum. Meth.* B **28** 135; see also Bermejo F J, Batallan F, Martinez J L, Garcia-Hernandez M, Enciso E and Alonso J 1990 *Europhys. Lett.* **12** 129
[21] Backus G and Gilbert F 1968 *Geophys. J. R. Astron. Soc.* **16** 169; for a concise description see Tarantola A 1987 *Inverse Problem Theory* (New York: Elsevier) p 461
[22] Bermejo F J, Ramirez R, Martinez J L, Batallan F and Prieto C to be published
[23] Lovesey S W 1985 *Z. Phys.* B **58** 79
[24] Bosse J, Jacucci G, Ronchetti M and Schirmacher W 1986 *Phys. Rev. Lett.* **57** 3277
[25] Potton J A, Daniell G J and Rainford B D 1986 *AERE Report* No. HL86/1237
[26] Backus G and Gilbert F 1970 *Phil. Trans. R. Soc. Lond.* **266** 126; see also 1967 *Geophys. J. R. Astron. Soc.* **13** 247
[27] Baumeister J 1987 *Stable Solutions of Inverse Problems* Vieweg Advanced Lectures in Mathematics (Braunschweig: Vieweg)